Multiple-scattering x-ray absorption analysis of quartzlike, rutilelike, and amorphous germanium dioxide

Erika Giangrisostomi,[1] Marco Minicucci,[1] Angela Trapananti,[2] and Andrea Di Cicco[1,3]
[1]*School of Science and Technology, Physics Division, University of Camerino, I-62032 Camerino, Italy*
[2]*CNR, IOM-OGG Grenoble, c/o European Synchrotron Radiation Facility, BP 220, F-38043 Grenoble Cedex, France*
[3]*IMPMC, Université Paris 6, CNRS, Campus Jussieu, F-75005 Paris, France*
(Received 27 April 2011; revised manuscript received 14 November 2011; published 6 December 2011)

The local structure of germanium dioxide, in its crystalline (quartzlike and rutilelike) and amorphous (a-GeO_2) solid phases, has been investigated by means of x-ray absorption spectroscopy (XAS). The short-range distance and angular distributions have been determined by modeling the experimental spectra with multiple-scattering contributions associated with selected n-body atomic configurations. Even for a-GeO_2, the experimental x-ray absorption signal ends up being significantly affected by the intra-tetrahedral (O-$\widehat{\text{Ge}}$-O) and inter-tetrahedral (Ge-$\widehat{\text{O}}$-Ge) angle distributions. Results from the present XAS structural refinements, including experimental determination of the local bond-angle distributions, are compared with previous experiments and molecular dynamics simulations.

DOI: 10.1103/PhysRevB.84.214202 PACS number(s): 61.05.cj, 61.43.Fs

I. INTRODUCTION

Germanium dioxide (GeO_2), otherwise referred to as germania, has been the focus of several investigations over the past years (Ref. 1 and references therein). The main motivations for these studies come from its peculiar optical properties and the fact that it is considered a chemical, and to a certain extent also a structural, analog of the geologically important silicon dioxide (SiO_2). Micoulaut *et al.* recently reviewed the current knowledge about the crystalline, amorphous, and liquid structures of GeO_2 as made known through a large variety of theoretical and experimental methods.[1] The former are mainly based on classical and *ab initio* molecular dynamics simulations while the latter encompass neutron and x-ray diffraction techniques as well as Raman, infrared, and nuclear magnetic resonance spectroscopies.

Various x-ray absorption spectroscopy (XAS) analysis of germania also exist,[2–8] yet often limited to the near-edge (XANES) region of the spectrum or concerned with the detection of the phase transformations that occur when increasing temperature or pressure. Most of the XAS studies have focused on the amorphous phase (a-GeO_2), which serves as a prototypical model to study oxide glasses. The crystalline quartzlike (q-GeO_2) and rutilelike (r-GeO_2) allotropic forms have been studied less extensively so that, to the authors' knowledge, the only structural information presently available is that coming from diffraction experiments.[9,10] Both for amorphous and crystalline GeO_2, the angular distributions are rarely mentioned, and when they are, their determination never comes from XAS experiments.

As is now well established, x-ray absorption spectroscopy is a probe of the local structure able to provide information on the second-, third-, and even higher-order correlation functions using multiple-scattering (MS) theory to model the x-ray absorption cross section. This approach has been implemented in the EXAFS (extended x-ray absorption fine structure) data-analysis package GNXAS,[12,13] particularly suited for disordered systems. Previous successful applications on amorphous Si[14] and Ge[15] indicate that accurate estimates of the structural parameters describing the pair and triplet distribution functions in crystalline and amorphous GeO_2, presently scattered and sometimes conflicting in the literature, are actually possible and can improve our knowledge about structural disorder and local vibrations in these materials.

The paper is organized as follows: A few details regarding the XAS experiments are given in Sec. II; subsections A, B, and C of Sec. III are devoted to discussing the results of the data analysis performed using the GNXAS method on q-GeO_2, r-GeO_2, and a-GeO_2, respectively; the main conclusions of the present work are drawn in Sec. IV.

II. EXPERIMENT

Well-characterized crystalline q-GeO_2 and r-GeO_2 have been obtained through the preparation methods described in Ref. 16. Vitreous GeO_2 (a-GeO_2) has been prepared by melting quartzlike GeO_2 at 1200 °C for about 17 hours and subsequently quenching it by immersion of the bottom of the host crucible in water. The absence of residual crystalline phases was checked by x-ray diffraction. We got samples for XAS measurements from appropriate amounts of germania, finely ground and homogeneously dispersed in graphite. The obtained powder mixtures were pressed to give pellets of optimal thickness for x-ray absorption measurements at the Ge K edge (∼11 103 eV).

The XAS experiments on q-GeO_2 and r-GeO_2 have been performed at the BM29 beamline of ESRF (Grenoble), while that on a-GeO_2 has been performed at the XAFS beamline of ELETTRA (Trieste). We refer the reader to Refs. 17,18 for a description of the two beamline layouts. The raw x-ray absorption data collected at ambient pressure and room temperature are reported in Fig. 1. Spectra were measured up to 1500 eV above the Ge K edge with a signal-to-noise ratio better than 10^4.

The glass spectrum closely resembles that of the quartzlike polymorph, which presents completely different features with respect to the spectrum of the rutilelike polymorph as a consequence of the different local structures. In fact, as widely recognized, the glassy state consists of

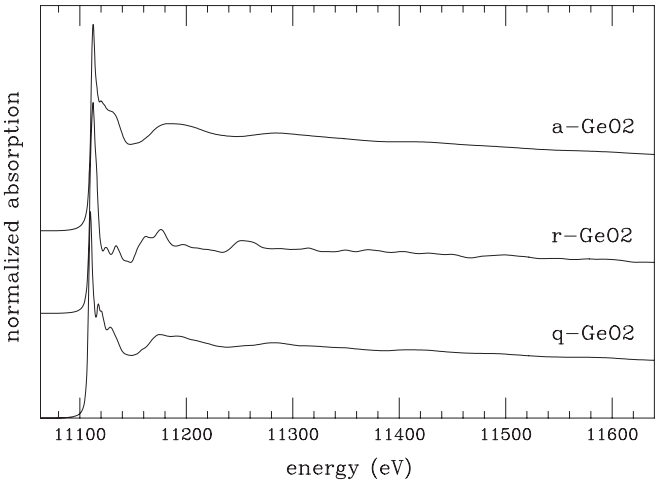

FIG. 1. Raw Ge K-edge x-ray absorption data for quartzlike (q-GeO_2), rutilelike (r-GeO_2), and amorphous (a-GeO_2) germanium dioxide.

four-coordinated germanium atoms in a corner-shared tetrahedral arrangement where bond lengths and angles are similar to those found in the quartzlike phase although giving rise to a structure that lacks long-range order. The rutilelike phase, instead, consists of sixfold-coordinated germanium atoms and threefold-coordinated oxygen atoms.

III. DATA ANALYSIS AND RESULTS

XAS data analysis has been carried out with the GNXAS package, according to the following procedure. Once a cluster reproducing the known structure on the basis of unit cell parameters provided by previous diffraction studies has been constructed, phase shifts were calculated for each nonequivalent atomic site within the cluster using the Hedin-Lundqvist approximation for the exchange-correlation part of the optical potential. Possible arrangements involving one, two, and three neighboring atoms have been identified—each corresponding to a peak of the pair (g_2), triplet (g_3), and quadruplet (g_4) distribution functions—and their contribution to the X-ray absorption cross section has been calculated by means of the continued-fraction algorithm.[11] Thermal and disorder effects have been accounted for and departures from the reference geometry have been allowed by evaluating the configurational average of each n-body absorption signal $\gamma^{(n)}$ over a Gaussian distribution function during the fitting procedure. This was aimed at minimizing the summed square residual between the experimental and theoretical signals, the construction of the latter involving a proper modeling of both the structural oscillations and the background.

A punctual evaluation of the statistical errors has also been performed. After calculating the Hessian matrix of the residual function in the minimum, statistical errors have been determined from the extension of 95% confidence intervals in two-dimensional contour plots, i.e., looking at the intersections between the ellipsoidal residual in the full parameter space and any two-parameter surface.

Full details about the methodology underlying GNXAS and applications to several liquids and glasses can be found in the literature.[12,13,19] XAS structural refinements for the three GeO_2 samples made use of a model for the background that, compatibly with previous investigations on Ge K-edge data (see for example Ref. 15), includes the opening of $1s$-$3d$ and $1s$-$3p$ double-electron excitation channels superimposed on a smooth polynomial curve. Nonstructural empirical parameters such as the overall amplitude correction factor (S_0^2) and the zero of the theoretical energy scale (E_0) were floated in a restricted range. S_0^2 resulted to be 0.93, 1.00, and 0.76 for q-GeO_2, r-GeO_2, and a-GeO_2, respectively, with an estimated error of about 5%. Correspondingly, E_0 turned out to exceed the energy edge (the point of the experimental spectrum with maximum first derivative) by 0.7, 0.2, and 10.4 eV.

A. q-GeO_2

Quartzlike germanium dioxide has a hexagonal unit cell containing three formula units. Ge and O atoms are positioned according to the $P3_221$ space group, the ones at the center and the others at the vertices of distorted tetrahedra.[9]

The short-range structure probed by XAS, up to a distance of about 3.4 Å around a photoabsorbing Ge atom, can be described through the following components: O and Ge first-shell atoms at distances R_1 and R_2 giving rise to the two-body signals $\gamma_1^{(2)}$ and $\gamma_2^{(2)}$, respectively; O-Ge-O triangular arrangements—made up of two Ge-O bonds forming, at the Ge site, the intra-tetrahedral angle θ_1—which originate the three-body signal $\gamma_1^{(3)}$; Ge-O-Ge triangular arrangements—here parametrized in terms of Ge-O and Ge-Ge first-shell distances and the angle θ_2 in between—which contribute to the x-ray absorption cross section through the three-body signal $\gamma_2^{(3)}$.

Best-fit signals from such pair and triplet configurations are shown in panel (a) of Fig. 2. The good agreement between the best-fit total calculated signal and the experimental one can be appreciated by looking at panel (b) of the same figure. The residual is mostly due to high-frequency contributions from atomic configurations involving farther atoms, as evident from the comparison in panel (c) of Fig. 2 between the moduli of the Fourier transforms in the real space.

Obtained values for the various structural parameters, along with estimated statistical error bars, are reported in Table I.

Our estimate of the mean Ge-O first-neighbor distance is halfway between the result of 1.7636 Å^2 from the density functional theory (DFT) study by Zwijnenburga *et al.*[20] and that from a similar study by Sevik *et al.*[21] reporting values of 1.693 and 1.699 Å. The Ge-O and Ge-Ge first-shell distances are more similar to those of 1.739 and 3.153 Å determined by Smith *et al.*[9] by means of x-ray diffraction. Both also compare quite well with the EXAFS determinations by Okuno *et al.*[2] yielding values of 1.738 and 3.151 Å, respectively. As for the bond-length variances, they end up being smaller and more different from one another with respect to those of 0.0050 and 0.0048 Å^2 reported in that previous EXAFS paper.

As confirmed by the molecular dynamics simulations presented by Oeffer *et al.*[22] at the temperature of 300 K it is not possible to distinguish between the slightly different

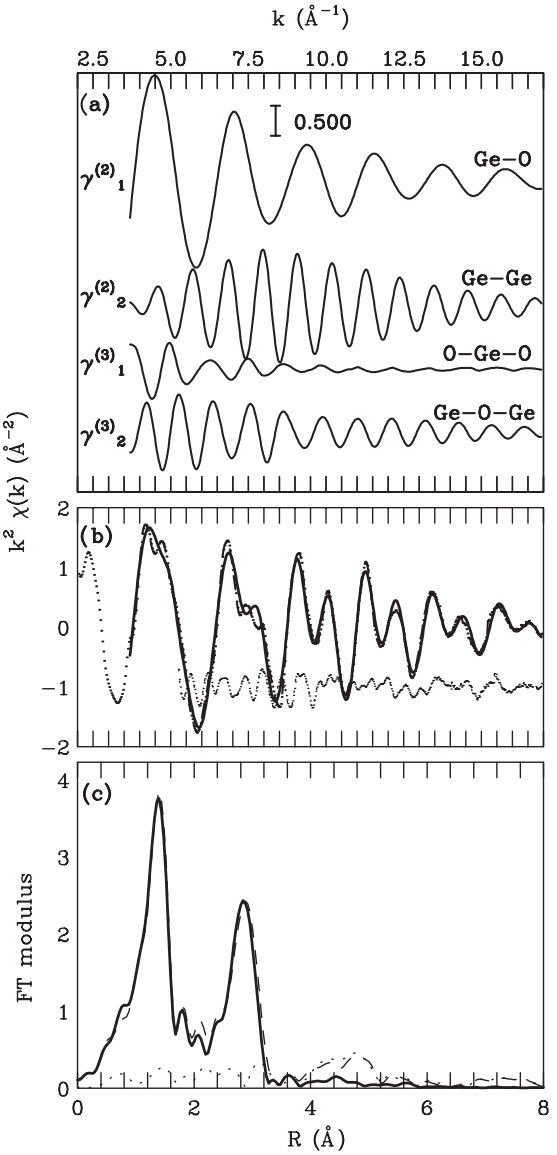

FIG. 2. XAS structural refinement of quartzlike germanium dioxide. (a) Two-body and three-body contributions to the Ge K-edge EXAFS of q-GeO_2 included in the fitting procedure. (b) Comparison between the experimental (dashed) and the total calculated (solid) EXAFS signals, with their difference indicated with a dotted curve. (c) Comparison between the Fourier transforms of the experimental (dashed) and the total calculated (solid) EXAFS signals, with the Fourier transform of the residual represented by a dotted curve.

O-$\widehat{\text{Ge}}$-O angles around the tetrahedral value (109.47°) that are predicted by crystallography. In this work we found that the O-$\widehat{\text{Ge}}$-O bond-angle distribution can be well approximated by a Gaussian function with mean value about 112° and variance 8°^{2}, which is compatible with a local structure made of vibrating distorted tetrahedra. Bond-bond and bond-angle correlations resulted in being negative, signifying that a reduction of one bond distance is accompanied by an average increase of the bond angle and of the neighboring bond distance, an effect which has been already observed in other covalent or close-packed systems.[13] The Ge-$\widehat{\text{O}}$-Ge distribution, where O is the oxygen atom shared between neighboring tetrahedra with centers in the two Ge atoms, is well reproduced using a mean angle that, at the Ge site, is equal to 26° (corresponding to about 128° at the O site). Its small variance and almost negligible correlation with the adjacent bond distances are indicative of a quite rigid inter-tetrahedral bond angle. A modest negative correlation is observed between the Ge-O lengths within a tetrahedron and the Ge-Ge lengths across nearby tetrahedra.

B. r-GeO_2

The polymorph of germanium dioxide which is isostructural with the stishovite allotrope of SiO_2, i.e., with the rutile allotrope of TiO_2, can be found under ambient conditions in a metastable state that is characterized by a tetragonal unit cell made of two molecules. Ge and O atoms are arranged according to the $P4_2/mnm$ spatial group, respectively at the center and at the vertices of distorted octahedra.

We built a cluster of atoms within a cutoff distance of 5.5 Å from the photoabsorber starting from the cell coordinates of Ref. 10 and using a tolerance parameter of 0.05 Å that allows us to treat the two inter-octahedron Ge-O bond lengths of 1.873 and 1.907 Å, for the four equatorial and the two axial bonds respectively, as making part of a single coordination shell. Nonetheless, this structure was found to give rise to a huge number of contributions to the pair, triplet, and quadruplet distribution functions (13, 53, and 69 peaks respectively). Therefore, we selected the most relevant two- and three-body configurations with which to build a model for the experimental spectrum according to the amplitude of the corresponding calculated EXAFS signals.

We found that, in order to reproduce the major features of the experimental spectrum up to about 4 Å, one must consider the atomic configurations described in the right half of Table I and generating the 9 signals shown in panel (a) of Fig. 3.

Structural parameters and absorption signals are classified as follows. R_1, R_4, R_5, and R_6 are the Ge-O first-, third-, fourth-, and fifth-shell average distances up to about 4.40 Å from the central Ge atom, and $\sigma^2_{R_1}$, $\sigma^2_{R_4}$, $\sigma^2_{R_5}$, and $\sigma^2_{R_6}$ are the corresponding variances. These parameters are associated with the two-body signals indicated as $\gamma^{(2)}_1$, $\gamma^{(2)}_4$, $\gamma^{(2)}_5$, and $\gamma^{(2)}_6$ in Fig. 3. R_2 and R_7 are the Ge-Ge first- and third-shell distances, and $\sigma^2_{R_2}$ and $\sigma^2_{R_7}$ are the corresponding variances. These parameters are associated with the two-body signals indicated as $\gamma^{(2)}_2$ and $\gamma^{(2)}_7$ in Fig. 3.

Similarly to the case of quartzlike germania, we also introduced two three-body configurations. The first one involves the Ge-$\widehat{\text{O}}$-Ge angle between two Ge-O first-neighbor bonds centered on the same Ge atom, whose mean value and variance are denoted as θ_1 and $\sigma^2_{\theta_1}$. This triangular arrangement gives rise to a three-body MS signal $\gamma^{(3)}_1$ but also automatically defines a Ge-Ge second-shell distance distribution. For this reason, following the terminology described in Refs. 12,13, we introduced in the best-fit procedure an effective-shell signal $\eta^{(3)}_1$, which is the sum of $\gamma^{(3)}_1$ and the two-body $\gamma^{(2)}_3$ signal arising from the long bond of the Ge-O-Ge triangle. In this way the structural refinement provided a measurement of the Ge-Ge second-shell average distance R_3 and of the corresponding variance $\sigma^2_{R_3}$.

TABLE I. Best-fit values for the structural parameters in q-GeO_2 and r-GeO_2. In the upper part, best-fit distances R and corresponding variances σ_R^2 and coordination numbers N (the latter kept fixed) taken into account in the XAS refinement. In the lower part, best-fit results for the two three-body configurations contributing to the XAS signals, each parametrized by an average angle θ, an angle variance σ_θ^2, a bond-bond ρ_{RR} correlation, a bond-angle $\rho_{R\theta}$ correlation, and a degeneracy deg (the number of equivalent three-body configurations). Roman numbers denote coordination shells, which are separately numbered for O and Ge atoms. Estimated statistical error bars on the last significant digits, corresponding to a 95% confidence interval, are indicated in parentheses for each parameter. When different from each other, upper (+) and lower (−) error bars are given separately. Only upper limits of the error bars are given when their lower limits coincide with physical constraints (zero for bond-length and angle variances). The + symbol next to the label Ge-O-Ge indicates that reported parameters for this triangular arrangement in q-GeO_2 refer to an angle measured at the Ge site (instead that at the O site). The ∗ symbol indicates that the Ge-Ge second-shell distance and error bars have been evaluated using the parameters defining the Ge-O-Ge triangular configuration.

	q-GeO_2				r-GeO_2			
		R (Å)	σ_R^2 (10^{-3} Å^2)	N		R (Å)	σ_R^2 (10^{-3} Å^2)	N
R_1	I Ge-O	1.730 (2)	2.1 (3)	4	I Ge-O	1.858(4)	3.0 (7)	6
R_2	I Ge-Ge	3.140 (3)	3.4 (3)	4	I Ge-Ge	2.88(1)	0.6 (+10)	2
R_3					II Ge-Ge *	3.42(2)	3 (1)	8
R_4					III Ge-O	3.45(4)	3 (+4)	4
R_5					IV Ge-O	3.90(5)	4 (+9)	8
R_6					V Ge-O	4.38(7)	3 (+15)	2
R_7					III Ge-Ge	4.41(5)	5 (−3 + 8)	4
		θ (°)	σ_θ^2 (°^{2})	ρ_{RR} $\rho_{R\theta}$ deg		θ (°)	σ_θ^2 (°^{2})	ρ_{RR} $\rho_{R\theta}$ deg
θ_1	O-Ge-O	111.5(6)	8 (7)	−0.5 (3) −0.7 (2) 6	Ge-O-Ge	134 (1)	3 (+5)	−0.5 (2) 8
θ_2	Ge-O-Ge$^+$	26.1(5)	1 (+1)	−0.2 (2) −0.1 (3) 4	Ge-O-O	0 (fixed)	4 (+4)	−0.7 (−3 + 7) 2

The second three-body configuration can be described in terms of the two Ge-O distances R_1 and R_6 and the null O-$\widehat{\text{Ge}}$-O angle in between, whose mean value θ_2 was kept fixed and whose variance σ_θ^2 was allowed to vary. With this triangular arrangement we associated the three-body MS signal $\gamma_2^{(3)}$ (not an effective-shell $\eta_2^{(3)}$ since the two two-body signals $\gamma_1^{(2)}$ and $\gamma_6^{(2)}$ were already considered separately). The extremal case of a collinear configuration resulting in intense multiple scattering signals is discussed in a previous paper.[13]

All correlations have been ignored, except that between the two Ge-O distances characterizing the first considered triangle, ρ_1, and that between the two Ge-O distances characterizing the second considered triangle, ρ_2.

The satisfactory agreement between the best-fit calculated and experimental EXAFS signals, presented together with their Fourier transforms in panels (b) and (c) of Fig. 3, demonstrates the effectiveness of our simplified model of the photoabsorber environment within about 4.5 Å, despite the complexity of the crystalline structure. The residual is basically only due to MS contributions related to atomic configurations at distances higher than 4.5 Å, the calculated signal reliably reproducing the experimental signal in the distance range covered by the calculations.

Best-fit parameters are reported in Table I. The mean Ge-O and Ge-Ge distances are in reasonable agreement with those of $R_1 = 1.872$–1.902 Å and $R_2 = 2.861$ Å obtained by single-crystal x-ray diffraction.[10] Discrepancies are larger at longer distances where EXAFS determinations are affected by larger errors because of the weaker signal intensities. We recall that a previous EXAFS experiment[4] yielded a mean Ge-O bond distance of 1.89 Å and farther Ge-Ge mean distances of 2.86 Å and 3.42 Å. For the distance variances only upper limits of the 95% confidence intervals are indicated in the table in those cases where their lower limits coincide with the physical zero constraint. Distance variances include both static and thermal disorder. The difference between the Ge-O and Ge-Ge first-shell distance variances seems to indicate that, while Ge-Ge distances are mainly affected by thermal broadening, Ge-O distances also suffer from substantial configurational disorder. For what concerns the three-body Ge-O-Ge and O-Ge-O configurations, in both cases we found quite narrow bond-angle distributions and negative bond-bond correlations. Such negative bond-bond correlations may be a consequence of the large static disorder affecting the first-shell Ge-O bond lengths as compared to the Ge-Ge first-neighbor distances.

C. a-GeO_2

The structure of amorphous germanium dioxide under ambient conditions has been studied in several previous works, whose achievements are schematically summarized in Table II. The various determinations for the structural parameters differ from one another and they sometimes do so quite substantially, as is the case with the bond-angle variances $\sigma^2_{\theta_{\text{O-Ge-O}}}$ and $\sigma^2_{\theta_{\text{Ge-O-Ge}}}$ which range (the first) from 23°^{2} to 38°^{2} and (the second) from 16°^{2} to 484°^{2}.

Our XAS analysis, which started from the same model structure as q-GeO_2, allowed us to characterize the pair and triplet correlation functions in this glass. The results of our best-fit refinement are shown in Figs. 4 and 5. The corresponding structural parameters are reported in the last row of Table II together with their statistical errors relative to a 95% confidence interval.

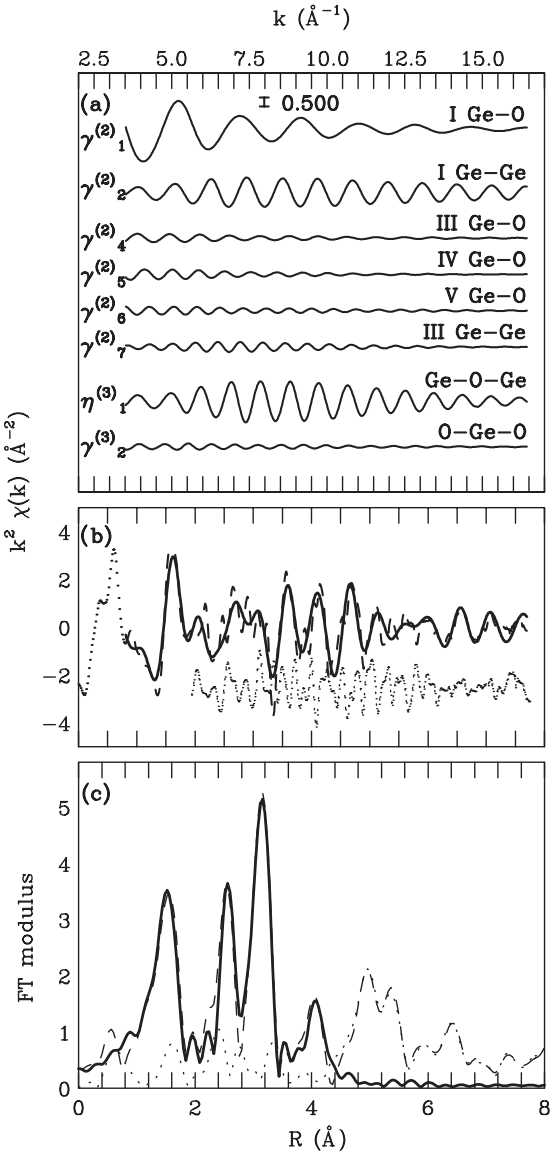

FIG. 3. XAS structural refinement of rutilelike germanium dioxide. (a) Two-body and three-body contributions to the Ge K-edge EXAFS of r-GeO_2 included in the fitting procedure. (b) Comparison between the experimental (dashed) and the total calculated (solid) EXAFS signals, with their difference indicated with a dotted curve. (c) Comparison between the Fourier transforms of the experimental (dashed) and the total calculated (solid) EXAFS signals, with the Fourier transform of the residual represented by a dotted curve.

The sensitivity of the x-ray absorption spectra to the shape of the three-body distributions is evident when we consider EXAFS calculations performed on the structural data resulting from the molecular dynamics (MD) simulation by Peralta *et al.*[32] that, using the very common potential developed by Oeffer and Elliott, predicted very broad bond-angle distributions. The signals related to such bond-angle distributions show a dramatic decrease in intensity, as seen in Fig. 4, in such way that the second peak of the Fourier-transformed EXAFS practically disappears, as seen in inset (d) of Fig. 5.

Panels (a), (b), and (c) of the same figure show that, by releasing the structural parameters far from their values in

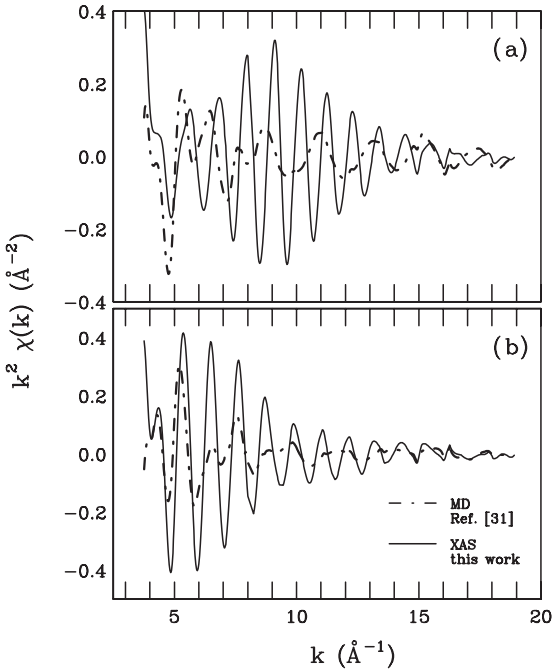

FIG. 4. Comparison between two models for the local structure of a-GeO_2. (a) Calculated EXAFS signal after subtraction of the contribution $\gamma_1^{(2)}$ from the first-shell of O atoms. (b) Calculated EXAFS signal after subtraction of the contributions $\gamma_1^{(2)}$ and $\gamma_2^{(2)}$ from the first shells of O and Ge atoms. Dot-dashed curves correspond to the structural parameters derived from the molecular dynamics simulation of Ref. 32, solid curves to the structural parameters resulting from our best-fit refinement of XAS data.

Ref. 32, a really excellent agreement is obtained between the calculated and experimental data. This demonstrates that our XAS data analysis is able to select between different models for the local structure of a-GeO_2 and thus provide an important tool for measuring changes in the local geometry of this system associated with different ordering levels.

The best-fit structural parameters reported in the last row of Table II are in line with previous results for what concerns the Ge-O and Ge-Ge first-shell distances. The Ge-O bond-length variance is similar to that of q-GeO_2, as reasonable, although smaller than found in a previous XAS work.[2] The Ge-Ge bond-length variance, instead, is much bigger than that of q-GeO_2, as an effect of the inter-tetrahedral angle disorder in glassy GeO_2.

The average O-$\widehat{\text{Ge}}$-O bond angle measured by us ends up being higher than other reported values while its variance stands at the lower limit of previous evaluations, its most probable value being 23°.

However, any value below 27° is acceptable within a 95% confidence interval. As for the Ge-$\widehat{\text{O}}$-Ge bond angle distribution, we can assess its average to settle to about 130°, a value very recurrent in the literature, and its variance to be less than 53°, with a most probable value of 23°. Such values, initially determined starting from the results $\theta_{\text{Ge–O–Ge+}} = 26°$ and $\sigma^2_{\theta_{\text{Ge–O–Ge+}}} < 8°^2$ for the angular distribution at the germanium site, have been verified to be consistent, within the quoted errors, with the results of a best-fit procedure that, starting from a different parametrization of the Ge-$\widehat{\text{O}}$-Ge

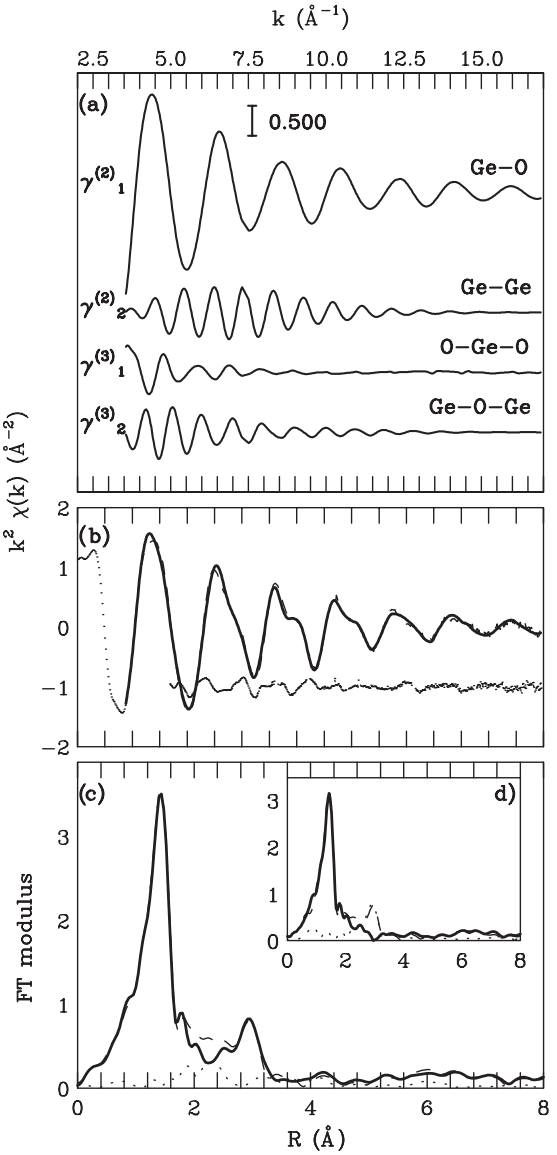

FIG. 5. XAS structural refinement of amorphous germanium dioxide. (a) Two-body and three-body best-fit contributions to the Ge K-edge EXAFS of a-GeO_2, analogous to those shown in Fig. 2 for a-GeO_2. (b) Comparison between the experimental (dashed) and the total calculated (solid) EXAFS signals, with their difference indicated with a dotted curve. (c) Comparison between the Fourier transforms of the experimental (dashed) and the total calculated (solid) EXAFS signals, with the Fourier transform of the residual represented by a dotted curve. (d) Comparison of the Fourier transform of the experimental EXAFS signal (dashed) with that (solid) calculated from the structural parameters yielded by the molecular dynamics simulation of Ref. 32.

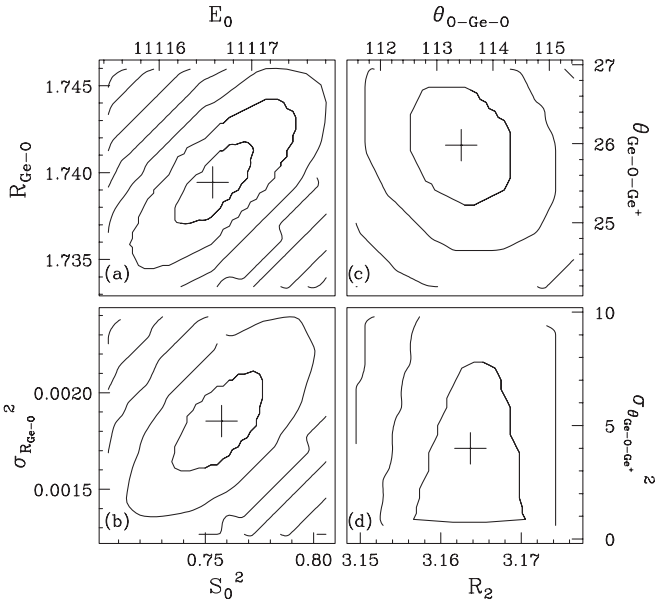

FIG. 6. Correlation maps between some fitting parameters for a-GeO_2 with inner curves representing 95% confidence intervals. (a) Ge-O first-shell distance (R_{Ge-O}) vs theoretical energy zero (E_0). (b) Ge-O first-shell distance variance ($\sigma^2_{R_{Ge-O}}$) vs amplitude correction factor (S_0^2). (c) Inter-tetrahedral angle at the Ge site ($\theta_{Ge-O-Ge+}$) vs intra-tetrahedral angle (θ_{O-Ge-O}). (d) Variance of the inter-tetrahedral angle at the Ge site ($\sigma^2_{\theta_{Ge-O-Ge+}}$) vs Ge-Ge first-shell distance (R_2).

bond-angle distribution, directly refines the angle at the oxygen site and its variance. These findings, if in fair agreement with those of Ref. 28 and not distant from those of Ref. 27, certainly do not support the MD studies cited in Table II.

For both three-body configurations, we found negligible bond-angle correlations. Bond-bond correlations, while also negligible for the Ge-O bonds belonging to adjacent tetrahedra, resulted in having a similar value as in the case of q-GeO_2 for the Ge-O bonds belonging to the same tetrahedron.

As was the case for q-GeO_2 and r-GeO_2, reported errors descend from a rigorous error analysis following the principles and methods illustrated in Refs. 33 and 19. As an illustrative example, we report in Fig. 6 contour plots between some of the most correlated parameters. The central crosses give the most probable values for each couple of parameters while from the extensions of the inner curves, representing the intersections of the 95% confidence interval with the chosen two-parameter subspaces, we deduced the corresponding errors. As we can see from panel (d), contour plots involving the variance of an angular distribution as one of the two parameters are far from having the expected elliptical shape. This is due to the fact that in these cases the 95% confidence interval reaches the zero physical constraint, representing the limit of absence of angular disorder. Thus, as we cannot associate a Gaussian distribution to the angle variances $\sigma^2_{\theta_{O-Ge-O}}$ and $\sigma^2_{\theta_{Ge-O-Ge+}}$, we have only reported upper bounds in Table II.

IV. CONCLUSIONS

In conclusion, we studied the short-range structure of germanium dioxide in its quartzlike, rutilelike, and amorphous forms through x-ray absorption spectroscopy at ambient conditions. By modeling the EXAFS signal with multiple scattering contributions from selected two- and three-body atomic configurations, our analysis provided a quantitative estimate of the structural parameters defining the pair and

TABLE II. Comparison of the results of the present EXAFS structural refinement with previous determinations of the local structure of amorphous GeO_2. The upper rows contain a summary of previous determinations by means of many different methods: XRD = x-ray diffraction, AXS = anomalous x-ray scattering, ND = neutron diffraction, NMR = nuclear magnetic resonance, vibr. spec. = first-principles analysis of vibrational spectra, MD = molecular dynamics, XAS = x-ray absorption spectroscopy. * = evaluated from published figures. The results obtained in this work are shown in the last row with the corresponding errors indicated in parentheses. ** = compatible with the parameters $\theta_{\mathrm{Ge-O-Ge+}} = 26.0(7)^\circ$ and $\sigma^2_{\theta_{\mathrm{Ge-O-Ge+}}} < 8^{\circ 2}$.

Reference	Method	$R_{\mathrm{Ge-O}}$ (Å)	$\sigma^2_{R_{\mathrm{Ge-O}}}$ (10^{-3} Å^2)	$R_{\mathrm{Ge-Ge}}$ (Å)	$\sigma^2_{R_{\mathrm{Ge-Ge}}}$ (10^{-3} Å^2)	$R_{\mathrm{O-O}}$ (Å)	$\theta_{\mathrm{Ge-O-Ge}}$ (°)	$\sigma^2_{\theta_{\mathrm{Ge-O-Ge}}}$ ($^{\circ 2}$)	$\theta_{\mathrm{O-Ge-O}}$ (°)	$\sigma^2_{\theta_{\mathrm{O-Ge-O}}}$ ($^{\circ 2}$)
23	XRD	1.74		3.18			133			
24	AXS	1.73		3.17		2.85	129–139			
25	AXS + ND	1.75		3.18		2.82				
26	AXS +XRD + ND	1.73		3.16		2.83	132			
27	XRD + ND	1.73		3.17			133	69		
28	NMR						130	16		
29	vib. spec.	1.78					135	112	109	36
30	MD	1.75		3.21		2.80	130	240*	108	23*
31	MD	1.69		3.21		2.78	133	158*	108	30*
32	MD	1.75	9*	3.26	47*	2.84	130	484*	109	38*
2	XAS	1.736	5.2	3.146	6.9		130			
This work	XAS	1.740(3)	1.8(3)	3.163(7)	7.7(7)		130(3)**	<53**	113.5(8)	<27

triplet distribution functions, the latter never investigated by previous XAS studies.

For crystalline quartzlike GeO_2, we measured a mean intra-tetrahedral O-$\widehat{\mathrm{Ge}}$-O angle of 111.5° with a variance of $8^{\circ 2}$, compatible with a local structure of vibrating distorted tetrahedra. The inter-tetrahedral Ge-$\widehat{\mathrm{O}}$-Ge angle, instead, was found to have a stiffer distribution. The more complicated structure of crystalline rutilelike GeO_2 was locally described in terms of only two three-body arrangements characterized by quite narrow bond-angle distributions. Also in the case of amorphous GeO_2, we revealed a significant contribution to the EXAFS signal from atomic sites beyond the first shell of oxygens neighbors. The most probable value of the intra-tetrahedral and inter-tetrahedral bond-angle variances resulted in being $23^{\circ 2}$, putting to the test some previous models for the short-range structure of this archetypal oxide glass. In particular, the lower Ge-$\widehat{\mathrm{O}}$-Ge bond-angle variance found in this work suggests that present modeling of inter-tetrahedral disorder in molecular dynamics simulations should be reconsidered.

Moreover, the data analysis here discussed represents an important basis for further EXAFS investigations of the densification mechanism in glassy germanium dioxide, largely debated in several recent works including a XAS study[7] where a continuous breakdown of the intermediate-range order upon increasing pressure has been suggested.

ACKNOWLEDGMENTS

D. de Ligny and C. Coussa-Simon (University Claude Bernard Lyon 1) are kindly acknowledged for having provided the q-GeO_2 and r-GeO_2 crystalline samples, prepared by P. Richet (IPG Paris) following the procedure described in Ref. 16. We also thank R. Cicconi and E. Principi (University of Camerino) for their help in the preparation of amorphous GeO_2 samples.

[1] M. Micoulaut, L. Cormier, and G. S. Henderson, J. Phys. Condens. Matter **18**, R753 (2006).
[2] M. Okuno, C. Yin, H. Morikawa, F. Marumo, and H. Oyanagi, J. Non-Cryst. Solids **87**, 312 (1986).
[3] B. Houser, N. Alberding, R. Ingalls, and E. D. Crozier, Phys. Rev. B **37**, 6513 (1988).
[4] J. P. Itié, A. Polian, G. Calas, J. Petiau, A. Fontaine, and H. Tolentino, Phys. Rev. Lett. **63**, 398 (1989).
[5] O. Ohtaka, A. Yoshiasa, H. Fukui, K.-i. Murai, M. Okube, Y. Katayama, W. Utsumi, and Y. Nishihata, J. Synchrotron Radiat. **8**, 791 (2001).
[6] L. Bertini, P. Ghigna, M. Scavini, and F. Cargnoni, Phys. Chem. Chem. Phys. **5**, 1451 (2003).
[7] M. Vaccari, G. Aquilanti, S. Pascarelli, and O. Mathon, J. Phys. Condens. Matter **21**, 145403 (2009).
[8] M. Baldini, G. Aquilanti, H.-k. Mao, W. Yang, G. Shen, S. Pascarelli, and W. L. Mao, Phys. Rev. B **81**, 024201 (2010).
[9] G. S. Smith and P. B. Isaacs, Acta Crystallogr. **17**, 842 (1964).
[10] W. H. Baur and A. A. Khan, Acta Crystallogr. Sect. B **27**, 2133 (1971).
[11] A. Filipponi, J. Phys. Condens. Matter **3**, 6489 (1991).
[12] A. Filipponi, A. Di Cicco, and C. R. Natoli, Phys. Rev. B **52**, 15122 (1995).
[13] A. Filipponi and A. Di Cicco, Phys. Rev. B **52**, 15135 (1995).
[14] A. Filipponi, A. D. Cicco, M. Benfatto, and C. R. Natoli, Europhys. Lett. **13**, 319 (1990).
[15] A. Filipponi and A. Di Cicco, Phys. Rev. B **51**, 12322 (1995).

[16]P. Richet, Phys. Chem. Miner. **17**, 79 (1990).
[17]A. Filipponi, M. Borowski, D. T. Bowron, S. Ansell, A. Di Cicco, S. De Panfilis, and J.-P. Itié, Rev. Sci. Instrum. **71**, 2422 (2000).
[18]A. Di Cicco, G. Aquilanti, M. Minicucci, E. Principi, N. Novello, A. Cognigni, and L. Olivi, J. Phys. Conf. Ser. **190**, 012043 (2009).
[19]A. Filipponi and A. Di Cicco, TASK Quarterly **4**, 575 (2000).
[20]M. A. Zwijnenburg, R. Huenerbein, R. G. Bell, and F. Corá, J. Solid State Chem. **179**, 3429 (2006).
[21]C. Sevik and C. Bulutay, J. Mater. Sci. **42**, 6555 (2007).
[22]R. D. Oeffner and S. R. Elliott, Phys. Rev. B **58**, 14791 (1998).
[23]A. Leadbetter and A. Wright, J. Non-Cryst. Solids **7**, 37 (1972).
[24]P. Bondot, Phys. Status Solidi A **22**, 511 (1974).
[25]Y. Waseda, K. Sugiyama, E. Matsubara, and K. Harada, Mater. Trans., JIM **32**, 421 (1990).
[26]D. L. Price, M.-L. Saboungi, and A. C. Barnes, Phys. Rev. Lett. **81**, 3207 (1998).
[27]J. Neuefeind and K.-D. Liss, Berichte der Bunsengesellschaft für physikalische Chemie **100**, 1341 (1996).
[28]R. Hussin, R. Dupree, and D. Holland, J. Non-Cryst. Solids **246**, 159 (1999).
[29]L. Giacomazzi, P. Umari, and A. Pasquarello, Phys. Rev. Lett. **95**, 075505 (2005).
[30]T. Li, S. Huang, and J. Zhu, Chem. Phys. Lett. **471**, 253 (2009).
[31]V. V. Hoang, J. Phys. Condens. Matter **18**, 777 (2006).
[32]J. Peralta, G. Gutiérrez, and J. Rogan, J. Phys. Condens. Matter **20**, 145215 (2008).
[33]A. Filipponi, J. Phys. Condens. Matter **7**, 9343 (1995).